Automated BIM-Ready 3D Reconstruction from Muon Flux Tomography Data: An IFC-Based Integration Pipeline for Bridge Inspection

Soheila Kooakalani[1], Ioannis Brilakis[1], Sander Sein[2], Tengiz Pataraia[2], Ya Wen[1], Mudan Wang[1], Xiaofang Wen[1]

[1]Department of Engineering, University of Cambridge, Cambridge CB3 0FA, UK.
[2]GScan Ltd, The Bradfield Centre, 184 Cambridge Science Park, Milton Road, Cambridge CB4 0GA, UK.
sk2268@cam.ac.uk, ib340@cam.ac.uk, sander.sein@gscan.eu, tangiz.pataraia@gscan.eu, yw710@cam.ac.uk, mw923@cam.ac.uk, xw436@cam.ac.uk

Abstract –

Ageing bridge infrastructure requires scalable, accurate, and minimally intrusive inspection methods that can reveal subsurface conditions while producing outputs compatible with digital engineering workflows. Muon Flux Technology (MFT) enables passive, non-destructive internal imaging of reinforced concrete elements, producing high-value geometric outputs that can support infrastructure inspection and asset management. A persistent barrier to operational deployment is the limited interoperability between processed MFT-derived outputs and standard Building Information Modelling (BIM) ecosystems. This paper presents a deterministic, programmatic pipeline that converts processed MFT-derived geometries into Industry Foundation Classes 4 (IFC4)-compliant models using a geometry-to-IFC tessellation workflow. Each detected object is provided as an individual Polygon File Format (PLY) file containing either a triangle mesh or a point cloud. Where only point data are available, the workflow reconstructs a surface via Ball Pivoting, applies mesh cleaning for topological stability, and exports the result as an IFC4 tessellated shape. A minimal IFC spatial hierarchy (Project-Site-Building-Storey) is authored to ensure broad compatibility across BIM tools and consistent unit handling. The resulting IFC outputs enable downstream coordination, archival, and integration of MFT-derived 3D information within open BIM workflows, supporting objectives related to data conversion, automation, integration, and standards compliance.

Keywords –

Muon tomography; Non-destructive testing; BIM integration; IFC; Bridge inspection.

1 Introduction

Ageing bridge infrastructure requires inspection methods that can reveal internal condition while minimizing traffic disruption and intrusive testing. Conventional non-destructive testing (NDT) methods, such as ground-penetrating radar, X-ray, and ultrasound, often face practical limitations such as limited penetration depth, operational complexity, cost, and restricted integration into digital workflows. Surface-based capture is widely adopted but does not provide subsurface insight critical for reinforced concrete condition assessment.

Muon Flux Technology (MFT) provides a complementary sensing modality. Muon-based imaging supports 3D internal imaging and can enable detection of internal features such as steel element geometry, voids, and other anomalies by measuring naturally occurring atmospheric muons and their scattering or attenuation through objects.

The M-TABS project aims to advance muon flux tomography for bridge assessment and to incorporate the resulting information stream into established formats such as 3D Building Information Modelling (BIM), thereby enabling integration into broader infrastructure maintenance practices. In this context, the paper addresses the automated conversion of processed MFT-derived outputs into BIM-compatible representations using industry-standard data formats [1]. Although the broader MFT-to-BIM vision is intended for bridge inspection in operational settings, the present paper focuses specifically on the deterministic conversion of processed MFT-derived geometries into IFC4-compliant BIM outputs. Accordingly, validation in this study is limited to processed data generated under simulation-based and controlled specimen conditions.

Recent work on construction digital transformation increasingly positions scan-to-BIM and digital twins as enabling layers for maintenance-focused decision support, where interoperability and traceable data exchange are recurring challenges [2–6]. Artificial intelligence (AI) techniques, including machine learning and deep learning, have been increasingly adopted to support automated analysis, prediction, and representation learning in complex engineering workflows [7–11]. Scan-to-BIM pipelines that convert reality-capture point clouds into semantic BIM have rapidly evolved from rule-based modelling to AI-assisted segmentation and automated Industry Foundation Classes (IFC) generation, and recent syntheses provide conceptual frameworks and best-practice guidance for reproducible adoption [12]. In parallel, the release of domain-specific datasets and benchmarks is beginning to standardise evaluation of scan-to-BIM methods and support generalisable learning-based approaches.

Beyond general reviews, open-source and benchmark-validated pipelines have been proposed to accelerate large-scale point-cloud-to-IFC conversion [13]. Domain-specific work has also demonstrated automated IFC generation for infrastructure assets such as railways by combining topology priors, parametric assemblies, and mesh-based reconstruction [14], and semi-automated IFC bridge modelling from point clouds has been explored for maintenance-oriented workflows [15]. Complementary efforts and related venues report deep learning-based Scan-to-BIM frameworks capable of reconstructing complex indoor elements from incomplete point clouds, underlining the continued push toward higher automation and robustness [16].

Muon imaging offers a complementary, passive modality for probing internal steel and density anomalies. It has demonstrated feasibility for reinforced concrete specimens and rebar-scale targets [17,18]. Yet, practical uptake in the built environment depends not only on reconstruction quality, but also on integrating outputs into established information-management ecosystems.

A key research gap therefore lies in the information integration layer: muon-tomography reconstructions are naturally produced as volumetric grids, point clouds or triangle meshes that are not readily expressible as parametric BIM objects and there is limited guidance on representing such internal, irregular geometries in openBIM formats while preserving metric integrity, provenance, and auditability. Although IFC4 supports tessellated geometry via IfcTessellatedFaceSet/IfcTriangulatedFaceSet for exchanging meshes in a standards-compliant manner [19], the use of these representations for NDT-derived internal reconstructions remains underexplored.

This paper addresses that gap by providing a deterministic Polygon File Format (PLY)-to-IFC4 conversion workflow for MFT outputs, designed to be reproducible and standards-compliant. The novelty is in (1) targeting subsurface muon-tomography reconstructions rather than surface scan-to-BIM, (2) encoding internal steel geometries and deviation maps using IFC tessellation to enable tool-agnostic exchange, and (3) emphasising auditability through explicit units, consistent spatial structure, and repeatable processing steps aligned with downstream inspection and digital-twin workflows. The main contributions are as follows: A deterministic, programmatic PLY-to-IFC4 conversion pipeline that supports both triangle meshes and point clouds; A robust preprocessing strategy, including surface reconstruction for point clouds, and mesh cleaning for stable IFC tessellation; Standards-based IFC export within a minimal IFC spatial structure, with explicit unit definition to prevent scaling ambiguity.

2 Background and Motivation

MFT uses naturally occurring muons in background radiation to compare incoming and outgoing particle distributions after they pass through a target. Variations in attenuation and scattering reveal internal geometry and material characteristics. Combined with AI-based reconstruction and classification, MFT enables subsurface 3D inspection for identifying embedded steel properties, cross-sections, and defects such as corrosion, voids, and cracking, as outlined in Table 1 against XRF. In the M-TABS project, this approach is applied to reinforced concrete bridge components, with the goal of producing 3D BIM outputs that fit existing inspection and asset-management workflows for operators and infrastructure owners. Figure 1 presents the GScan muon flux detector hardware used to collect the measurement data in this study. Muons are generated when cosmic rays interact with the atmosphere and, due to their high mass, can penetrate significant thicknesses of materials such as steel and concrete. In MFT, the process involves measuring the incoming particle flux, observing how particles are scattered or absorbed as they pass through an object, and measuring the exiting flux and scattering features such as $\Delta\theta$. These measurements are then used with AI to reconstruct internal structures and infer material composition, as different materials produce distinct attenuation and scattering signatures, as illustrated in Figure 2. A key technical challenge is converting tomography-native outputs into BIM-native representations. Tomography generates voxel-based or unstructured geometric data, while BIM represents structured, semantic objects within a spatial hierarchy. IFC, as the main interoperability standard, uses tessellated geometry in IFC4 to encode irregular surfaces as triangulated meshes, preserving geometric fidelity and compatibility with BIM tools, but with reduced parametric flexibility and larger file sizes.

Table 1 Comparison of XRF and muon tomography + AI across key operational criteria.

Criterion	XRF	Muon
Penetration depth	Limited	~10 m
Ability to penetrate shielded materials	Moderate	High
Chemical composition identification	Yes	Yes
Material agnostic / number of materials	High	Very high
Scanning time per m³	Rapid	Extended
Environmental insensitivity	Very low	High
System size / portability	Portable	1.75 × 0.75 m
Resolution / accuracy	Millimetre-scale	~1 mm

Figure 1. muon flux detector hardware.

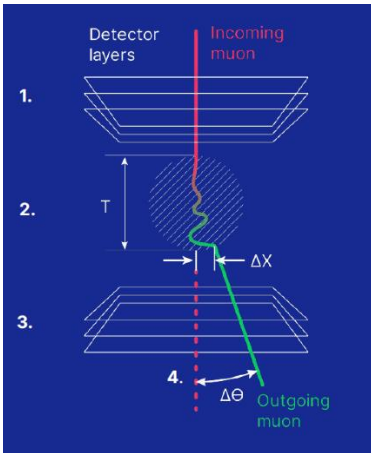

Figure 2. Muon tomography imaging principle.

3 Process Context and interdependencies

3.1 Data Acquisition

The first step establishes the foundational data assets required for method development and benchmarking across the project by creating a simulation-based dataset derived from an infrastructure asset. In addition to generating representative synthetic measurements, this step is explicitly responsible for delivering (1) a Universal Simulation Environment and (2) a Benchmark Data Library that provide consistent, controlled inputs for subsequent development and validation in the following steps. In practical terms, first step outputs must support two complementary needs: (a) physics-consistent scene and sensor configuration to enable reproducible simulation studies, and (b) ground-truth geometric or volumetric representations that can be used to benchmark reconstruction fidelity, segmentation accuracy, and downstream model conversion. The attached artefacts exemplify these two output classes: Simulation environment or scene definition, Benchmark volumetric ground truth. Overall, first step outputs operationalize the project's data-first dependency chain: they enable second step to develop and validate processing algorithms under controlled conditions, and they provide the reference geometries and volumetric benchmarks that ultimately support conversion of processed outputs into interoperable BIM deliverables. Figure 3 provides an example first step benchmark environment and associated ground-truth geometry.

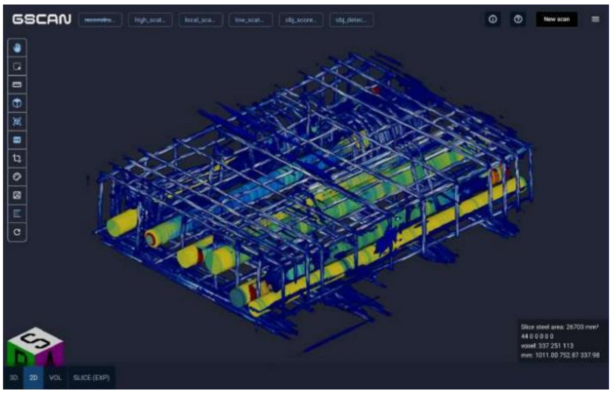

Figure 3. Simulation environment and benchmark volumetric ground truth.

3.2 Data Processing

The next step focuses on transforming muon-derived reconstructions into engineering-consumable, object-level outputs that can be directly ingested by downstream BIM integration workflows. In addition to improving the quality and usability of processed results, second step provides the intermediate representations required for

IFC generation: (1) classified material outputs, (2) instance-level segmentation of reinforcement, and (3) geometry and location descriptors suitable for object placement and semantic assignment. The outputs illustrate a concrete processing chain starting from a volumetric steel representation and culminating in object-level data products: Voxel-to-point conversion and material classification: A vowelized MFT volume is converted into a point-based (PLY) format and classified by material (e.g., concrete and rebar), producing the basic candidate point clouds required for further modelling and export. In the voxel-to-point conversion stage, each retained voxel was represented by a single point located at its centroid. This choice provides a compact object-level representation for downstream classification and export, but it also smooths boundary detail relative to explicit voxel-surface extraction. Consequently, the final mesh quality depends on the voxel resolution and on the subsequent surface reconstruction stage, which together govern the trade-off between data compactness and geometric fidelity. Representative outputs from this conversion and classification step are shown in Figure 4.

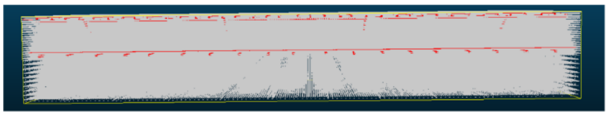

(a)

(b)

(c)

Figure 4. Voxel-to-point conversion and material classification outputs from MFT-derived volumes: (a) Point cloud; (b) Concrete classification; (c) Rebar classification.

Instance segmentation to isolate individual rebars: This stage evaluates multiple geometric instance segmentation methods to extract individual rebars from classified point clouds, a prerequisite for correct IFC export. Density-Based Spatial Clustering of Applications with Noise (DBSCAN) leads to over-segmentation, cylinder fitting under-detects rebars, and region growing improves detection but still suffers from fragmentation and missed elements. Overall, these results show that purely geometric approaches struggle with connected, irregular, or partially observed rebars, limiting reliable one-object-per-element IFC generation. This limitation is important for the downstream IFC conversion stage. The geometry-to-IFC workflow assumes that each input PLY corresponds to a single, correctly isolated physical object. Therefore, when upstream segmentation produces merged rebars, fragmented instances, or incomplete separations, the downstream export does not resolve these errors; instead, it deterministically converts the provided geometry into a tessellated IFC element. In this sense, segmentation quality directly governs semantic reliability, object granularity, and the engineering interpretability of the resulting BIM model. Figure 5 illustrates representative qualitative results of instance segmentation.

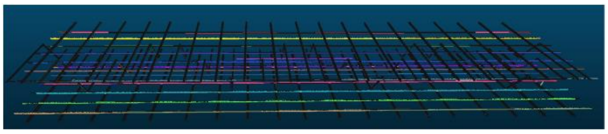

Figure 5. Instance segmentation of steel data.

Few-shot learning-based instance segmentation: This method is introduced to address the limitations of purely geometric approaches, trained on a small manually labelled rebar dataset. This approach improves isolation of individual rebars and more robustly handles connected and irregular shapes, enabling consistent object-level outputs suitable for BIM/IFC generation. A representative output from the few-shot approach is shown in Figure 6.

Although quantitative instance segmentation metrics such as Intersection over Union (IoU), Precision, Recall, and F1-score would strengthen the upstream evaluation, they are not reported in this study because no benchmark dataset with ground-truth instance labels was available for this stage of the MFT processing pipeline. The segmentation assessment is therefore presented qualitatively, with emphasis on the observed failure modes of geometric methods, including over-segmentation, fragmentation, and missed elements, and on the improved object isolation achieved by the few-shot learning approach. Establishing a benchmark dataset with instance-level ground truth remains an important next step for rigorous quantitative evaluation of segmentation performance. Geometry information extraction for downstream modelling: extracts per-instance geometric and location attributes into a structured tabular format, producing instance-level descriptors that support semantic classification, spatial placement, validation, and auditability in downstream BIM/IFC workflows.

Collectively, these outputs provide the two key input families required for IFC authoring: Object-level geometries, including one PLY per segmented rebar instance and meshes derived from those instances, and Instance metadata that support semantic assignment and consistent placement.

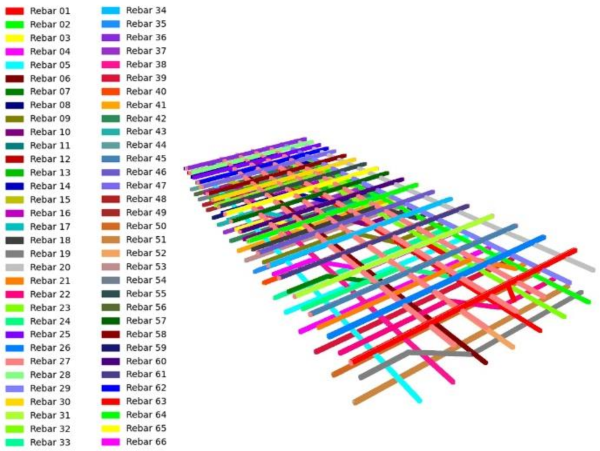

Figure 6. Few-shot learning-based instance segmentation result.

3.3 3D Model Generation and BIM Integration

The next step converts processed outputs into BIM-compatible 3D representations and ensures the resulting models adhere to industry standards for data exchange and integration. Its objectives include (1) data conversion to BIM-compatible formats, (2) automation of 3D model generation from processing outputs, (3) integration into BIM software for accurate 3D representations, and (4) standards alignment for model generation and exchange. The deliverable of this step is an updated front-end for GScan's MFT, which consumes outputs from the previous steps and supports downstream pilot implementation and evaluation in later steps. This paper addresses a specific and critical third step capability: open-standard IFC4 generation from processed, object-level geometries (exported as PLY). The presented methodology implements a deterministic, programmatic geometry-to-IFC tessellation workflow using IFC4 constructs to maximize interoperability.

The third step consumes the output of the second step in the form of per-object geometry files, PLY point clouds and reconstructed meshes for individual reinforcement instances, along with associated instance-level geometry and location descriptors**.** These artefacts enable a direct, automated export pathway: each segmented instance is converted into a discrete IFC element, represented using IFC4 tessellated geometry (IfcTriangulatedFaceSet) and inserted into a minimal IFC spatial hierarchy with explicitly units (metres).

4 Methodology: IFC generation method

The IFC model was generated through a deterministic, programmatic geometry-to-IFC tessellation workflow. Processed MFT-derived geometries were converted into BIM-compatible objects by constructing a minimal IFC spatial hierarchy and embedding each object's surface representation as an IFC4-compliant tessellated shape. The implementation used Open3D for geometry handling and IfcOpenShell for IFC authoring.

Each input object was provided as an individual PLY file that may contain either (1) a triangle mesh (faces + vertices) or (2) a point cloud (vertices only). For each PLY:

Mesh detection: The file was first read as a triangle mesh. If valid faces were present, the mesh was used directly.

Surface reconstruction (point clouds only): When no faces were present, the point cloud was converted into a triangle mesh using Ball Pivoting Surface Reconstruction. Surface normals were estimated prior to reconstruction. For a point cloud with N points, the average nearest-neighbor spacing was computed as:

$$\bar{d}_{nn} = \frac{1}{N}\sum_{i=1}^{N} d_i^{nn} \tag{1}$$

where d_i^{nn} is the Euclidean distance from point i to its nearest neighboring point. The Ball Pivoting radii were then defined as:

$$R = \{k_1\bar{d}_{nn}, k_2\bar{d}_{nn}, k_3\bar{d}_{nn}\} \tag{2}$$

where k_1, k_2, and k_3 are fixed scale multipliers used consistently across the dataset. In our implementation, $k_1 = [1.5]$, $k_2 = [2.5]$, and $k_3 = [3.5]$. This radius-selection strategy preserves geometric scale consistency across point clouds with different sampling densities.

Mesh cleaning: The resulting mesh (either imported or reconstructed) was cleaned using standard topological repairs, including removal of duplicated and degenerate triangles, non-manifold edge mitigation, and recomputation of vertex normal, to ensure stable downstream tessellation.

A valid IFC4 container structure was created to ensure compatibility with standard BIM tools. The following spatial entities were instantiated: IfcProject (root), IfcSite, IfcBuilding, and IfcBuildingStorey. Length units were explicitly assigned as meters in "UnitsInContext" to prevent viewer-dependent scaling issues. This structure provides the minimum required context so that imported elements appear correctly in IFC viewers and BIM authoring platforms.

Each mesh was encoded as IFC tessellated geometry using IfcTriangulatedFaceSet, which is the IFC4 entity intended for representing arbitrary triangular surfaces: Mesh vertices were written to IfcCartesianPointList3D (CoordList), preserving the original coordinate system after any required scaling or normalisation. Mesh faces were written to IfcTriangulatedFaceSet (CoordIndex), as illustrated in Figure 7 [19]. Because IFC indexing is 1-based, face indices were shifted accordingly during export.

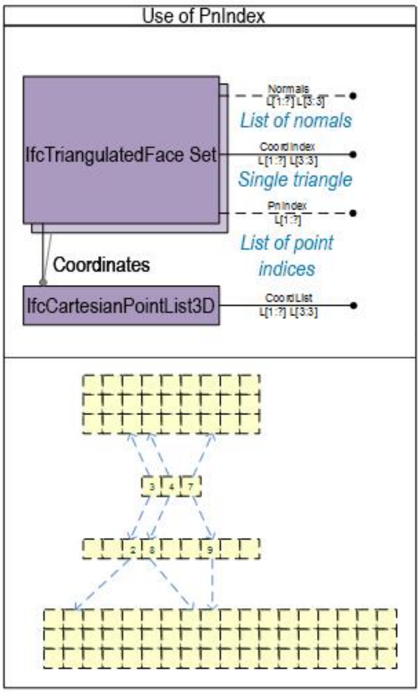

(a)

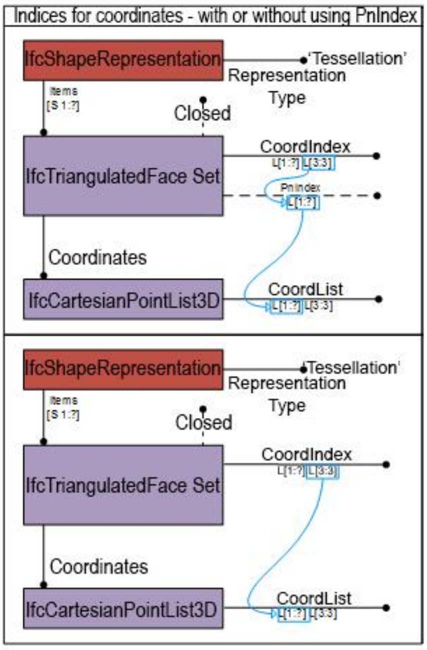

(b)

Figure 7. (a) IfcCartesianPointList3D; (b) IfcTriangulatedFaceSet.

The tessellated geometry was placed into a standard shape representation: (1) IfcShapeRepresentation with: RepresentationIdentifier = "Body", RepresentationType = "Tessellation", Items = [IfcTriangulatedFaceSet]; (2) Wrapped in IfcProductDefinitionShape and assigned to the element's Representation. This approach produces broad interoperability across IFC viewers. For each exported object, an IFC product instance was created and inserted into the spatial structure: (1) Element class assignment: Objects were exported either as IfcReinforcingBar (when the object corresponded to rebar) or as a generic IfcBuildingElementProxy when semantic classification was not available or not required; (2) Placement: Each element was assigned an IfcLocalPlacement (default orientation and origin placement, or a project-defined local reference frame if applied); (3) Containment: Elements were associated with a bridge-relevant spatial container, including IfcBridge and IfcFacilityPart, via IfcRelContainedInSpatialStructure, ensuring correct visibility, hierarchy, and navigation within BIM and digital engineering environments.

5 Results and Discussion

The exported IFC contains a valid spatial hierarchy, one IFC product per input PLY object, a tessellated body representation for each object, and consistent placement, ensuring that the objects appear as expected in standard BIM viewers. The symmetric Chamfer distance between each input geometry and the tessellated geometry re-extracted from the exported IFC was used to assess geometric fidelity. The average Chamfer mean was 0.61 mm, and the average Chamfer p95 was 2.53 mm. When the input was already a mesh, the export was effectively lossless, with a mean Chamfer distance of 0.02 mm and a p95 of 0.09 mm, confirming high-fidelity tessellation-based IFC encoding. For point-cloud inputs requiring Ball Pivoting reconstruction, the average errors increased to a mean of 1.20 mm and a p95 of 4.97 mm, indicating that the dominant source of error arises from surface reconstruction rather than from the IFC encoding itself. In terms of efficiency, end-to-end processing averaged 2.60 s per element. The exported IFC size was 27,774 KB, indicating that the conversion achieves interoperability with only a modest increase in file size. For rebar-representative objects, IfcReinforcingBar provides a semantically meaningful class assignment; otherwise IfcBuildingElementProxy ensures a safe fallback without overstating semantics. While this export strategy provides a robust and conservative pathway for geometry-to-IFC conversion, the present implementation offers only limited semantic enrichment. The current BIM output primarily encodes geometry, placement, and basic class assignment, and does not yet attach richer property information such as reconstruction confidence, uncertainty bounds, estimated bar diameter, or provenance metadata from the upstream MFT processing stages. As a result, the exported model is currently more suitable for visualization, exchange, coordination, and auditability than for advanced engineering querying or asset-management analytics. Future work should therefore extend the exported entities with infrastructure-relevant property sets and provenance-aware metadata once such attributes can be derived and validated consistently. Figure 8 shows a representative exported model visualised in Autodesk Revit and AutoCAD. The reported results therefore demonstrate the feasibility of standards-compliant geometry-to-IFC conversion under controlled inputs, but they should not yet be interpreted as full evidence of robustness under active bridge operating conditions.

A practical challenge in processing muon-derived outputs is variability in representation: some objects may be exported as watertight meshes, while others may be sparse point clouds. The two-path approach (direct mesh handling vs deterministic surface reconstruction) addresses this variability while maintaining a single IFC export strategy. Mesh cleaning is critical: repairing degenerate triangles and mitigating non-manifold conditions substantially reduces the likelihood of unstable or invalid tessellation in downstream BIM tools. The use of IfcTriangulatedFaceSet was chosen for robustness and compatibility with irregular MFT-derived geometries, but it may be inefficient for large infrastructure models because high-resolution meshes can increase file size and reduce viewer performance. The paper should therefore state that this choice prioritizes reliable geometry preservation over efficiency, while noting that future work will explore parametric rebar modelling, mesh decimation, and level-of-detail control to improve scalability.

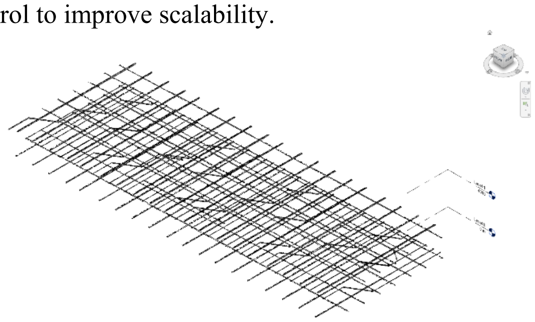

(a)

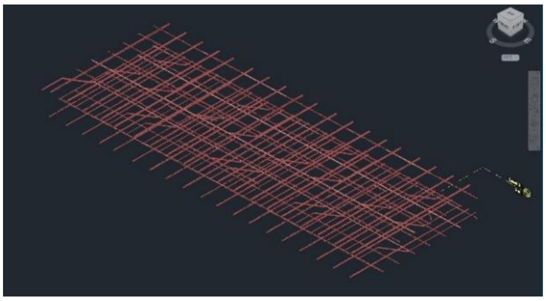

(b)

Figure 8. Representative exported IFC visualized in: (a) Revit; (b) AutoCAD.

6 Conclusion

This paper presented an IFC generation method that converts processed MFT-derived geometries, including PLY meshes and point clouds, into IFC4-compliant BIM deliverables through a deterministic geometry-to-IFC tessellation workflow. Using Open3D for geometry handling and IfcOpenShell for IFC authoring, the approach constructs an IFC spatial hierarchy, explicitly defines meter units, and exports each object as a standard Body/Tessellation representation using IfcTriangulatedFaceSet. The result is a robust, interoperable pathway for integrating muon-derived 3D information into open BIM workflows, supporting objectives related to data conversion, automation, integration, and standards compliance.

An important next step is validation using data acquired from an actively operating bridge, where operational noise, environmental variability, attenuation uncertainty, and site constraints may affect the reliability of the broader pipeline. Future work can extend this foundation in four directions: (1) Richer semantic mapping: expanding beyond IfcReinforcingBar and proxy entities to additional infrastructure-relevant classes and property sets, including provenance metadata and confidence descriptors where available from upstream processing; (2) Parametric reconstruction when feasible: for objects approximating canonical forms, such as cylindrical reinforcement, exporting swept solids or other parametric representations alongside tessellated geometry to improve editability and downstream analytics; (3) Scalability optimization: introducing mesh decimation strategies and level-of-detail management to control file size and improve import performance for large-scale scans; (4) Infrastructure-specific spatial context: where project requirements demand, align the spatial structure with bridge/facility conventions and integrate with wider asset information containers.

Acknowledgement

The financial support of Innovate UK under the project "Muon Tomography for Assessing Bridge Structures" (Project Reference: 10132366) and the D-HYDROFLEX project under the European Union's Horizon Program (Grant Agreement No. 101122357) is gratefully acknowledged.

References

[1] S. Kookalani, E. Parn, I. Brilakis, S. Dirar, M. Theofanous, A. Faramarzi, M.A. Mahdavipour, Q. Feng, Trajectory of building and structural design automation from generative design towards the integration of deep generative models and

optimization: A review, Journal of Building Engineering 97 (2024) 110972. https://doi.org/10.1016/J.JOBE.2024.110972.
[2] M. Abdelrahman, E. Macatulad, B. Lei, M. Quintana, C. Miller, F. Biljecki, What is a Digital Twin anyway? Deriving the definition for the built environment from over 15,000 scientific publications, Build. Environ. 274 (2025) 112748. https://doi.org/10.1016/J.BUILDENV.2025.112748.
[3] W. Hu, Y. Ou, H. Liu, P. Ni, C. Chang, Integrating digital twin technologies for maintenance 4.0 in the building industry: A review and conceptual framework, Build. Environ. 288 (2026) 113997. https://doi.org/10.1016/J.BUILDENV.2025.113997.
[4] H. Alavi, S. Kookalani, F. Rahimian, N. Forcada, Integrated Building Intelligence, (2024). https://doi.org/10.1007/978-3-031-68865-2.
[5] S. Kookalani, S. Green, P. Luo, H. Alavi, E. Parn, Z. Sun, I. Brilakis, Mapping digital twin applications in infrastructure and the built environment across research types, methods, sectors, phases, and scales, Autom. Constr. 182 (2026) 106778. https://doi.org/10.1016/J.AUTCON.2026.106778.
[6] P. Luo, E. Parn, S. Kookalani, I. Brilakis, TailorAlert: Large Language Model-Based Personalized Alert Generation System for Road Infrastructure Management with Digital Twins, Computing in Civil Engineering 40 (2025). https://doi.org/https://doi.org/10.1061/JCCEE5.CPENG-7025.
[7] S. Kookalani, B. Cheng, S. Xiang, Shape optimization of GFRP elastic gridshells by the weighted Lagrange ε-twin support vector machine and multi-objective particle swarm optimization algorithm considering structural weight, Structures 33 (2021) 2066–2084. https://doi.org/10.1016/j.istruc.2021.05.077.
[8] S. Xiang, B. Cheng, S. Kookalani, An analytic solution for form finding of GFRP elastic gridshells during lifting construction, Compos. Struct. 244 (2020). https://doi.org/10.1016/j.compstruct.2020.112290.
[9] S. Kookalani, S. Nyunn, S. Xiang, Form-finding of lifting self-forming GFRP elastic gridshells based on machine learning interpretability methods, Structural Engineering and Mechanics 84 (2022) 605–618. https://doi.org/10.12989/sem.2022.84.5.605.
[10] H. Liu, H. Su, S. Kookalani, M. Cao, Y. Lei, W. Wu, Attention-enhanced spatiotemporal deep learning-based automatic warning model with uncertainty estimation in dam safety, Struct. Health Monit. (2025). https://doi.org/10.1177/14759217251358537.
[11] S. Kookalani, B. Cheng, J.L.C. Torres, Structural performance assessment of GFRP elastic gridshells by machine learning interpretability methods, Frontiers of Structural and Civil Engineering 16 (2022) 1249–1266. https://doi.org/10.1007/s11709-022-0858-5.
[12] E. Noroozinejad, A. Hajirasouli, G.M. Morrison, M. Kagioglou, J. Patil, M. Kalantari, Automatic Scan-to-BIM—The Impact of Semantic Segmentation Accuracy, Buildings 2025, Vol. 15, Page 1126 15 (2025) 1126. https://doi.org/10.3390/BUILDINGS15071126.
[13] S. Zbirovský, V. Nežerka, Open-source automatic pipeline for efficient conversion of large-scale point clouds to IFC format, Autom. Constr. 177 (2025) 106303. https://doi.org/10.1016/J.AUTCON.2025.106303.
[14] M.R.M.F. Ariyachandra, I. Brilakis, Leveraging railway topology to automatically generate track geometric information models from airborne LiDAR data, Autom. Constr. 155 (2023) 105068. https://doi.org/10.1016/J.AUTCON.2023.105068.
[15] Y. Schatz, B. Domer, Semi-automated creation of IFC bridge models from point clouds for maintenance applications, Front. Built Environ. 10 (2024) 1375873. https://doi.org/10.3389/FBUIL.2024.1375873/BIBTEX.
[16] M. Mahmoud, Z. Zhao, W. Chen, M. Adham, Y. Li, Automated Scan-to-BIM: A deep learning-based framework for indoor environments with complex furniture elements, Journal of Building Engineering 106 (2025) 112596. https://doi.org/10.1016/J.JOBE.2025.112596.
[17] E. Niederleithinger, S. Gardner, T. Kind, R. Kaiser, M. Grunwald, G. Yang, B. Redmer, A. Waske, F. Mielentz, U. Effner, C. Köpp, A. Clarkson, F. Thomson, M. Ryan, D. Mahon, Muon Tomography of the Interior of a Reinforced Concrete Block: First Experimental Proof of Concept, Journal of Nondestructive Evaluation 2021 40:3 40 (2021) 65-. https://doi.org/10.1007/S10921-021-00797-3.
[18] K. Doi, S. Hiromoto, T. Shinohara, al -, L. Chen, X. Liu, Y. Lin, S. Hiromoto -, M. Dobrowolska, J. Velthuis, A. Kopp, M. Perry, P. Pearson, Towards an application of muon scattering tomography as a technique for detecting rebars in concrete, Smart Mater. Struct. 29 (2020) 055015. https://doi.org/10.1088/1361-665X/AB7A3F.
[19] 8.8.3.47 IfcTriangulatedFaceSet - IFC4.3.2.0 Documentation, (2024). https://standards.buildingsmart.org/IFC/RELEASE/IFC4_3/HTML/lexical/IfcTriangulatedFaceSet.htm#Figure-8.8.3.47.B-Triangulated-face-set.